Superlattices and Microstructures 142 (2020) 106507

Contents lists available at ScienceDirect

Superlattices and Microstructures

journal homepage: www.elsevier.com/locate/superlattices

Study of oxygen plasma induced modulation of photoconductivity in MoS_2 field effect transistor

Muhammad Atif Khan [a], Servin Rathi [b], Sun Jin Yun [c], Gil-Ho Kim [b,*]

[a] Department of Electrical and Computer Engineering, Air University, Sector E-9, Islamabad, Pakistan
[b] School of Electronic and Electrical Engineering and Sungkyunkwan Advanced Institute of Nanotechnology (SAINT), Sungkyunkwan University, Suwon, 16419, South Korea
[c] ICT Components and Materials Technology Research Division, Electronics and Telecommunications Research Institute, Daejeon, 34129, South Korea

ARTICLE INFO

Keywords:
Oxygen plasma
2D material
MoS_2
Photoconductivity
Opto-electrical characteristics

ABSTRACT

We studied the effect of oxygen plasma treatment on the drain current and photoconductivity of the two dimensional few-layers MoS_2 based field-effect transistors (FETs). It was observed that the oxygen plasma can reduce the photoconductivity of MoS_2 channel along with variation in the current characteristics. This study shows the contribution of mild oxygen plasma to modulate the photoconductivity of the MoS_2 FETs which can have potential in optoelectronic detectors and sensors applications.

1. Introduction

Since the discovery of graphene, research in two-dimensional (2D) materials have grown exponentially, especially after the entry of the family of transition metal dichalcogenides (TMDCs) [1–3]. The unique electrical, optical and material properties of these TMDCs have been projected to replace various semiconductors in the near future. In this regard, the exploration of various properties of atomic thick TMDCs like molybdenum disulphide (MoS_2) for studying and modulating surface reactivity, doping, and defects formation through multifarious methods are subject of intense study [4–6]. One of such techniques is the plasma exposure of the TMDCs based devices for novel applications and transport studies. Of these surface modification methods, lattice-defects induced by the non-reactive plasma and its effect on various properties like photoluminescence (PL), carrier transport and doping are currently under study by many research groups [7–11].

In this work, we carried out the low energy oxygen plasma treatment on few layer MoS_2 FETs with back gate structure to study the effect on electrical and optoelectrical characteristics. Recently, several studies have been carried out to investigate the effect of plasma conditions on the optical properties like PL and Raman spectra [8,12,13], however the simultaneous study of crucial optoelectrical characteristics along with optical data has not been reported yet. Therefore, in this study, a detailed analysis of the effect of various plasma conditions on the optoelectrical characteristics was carried out. The results show that the optoelectrical characteristics agree well with observed optical quenching effect in PL and Raman scattering after plasma treatment. Such observation must be attributed to plasma induced defects in the lattice which can trap the photo-induced carriers resulting in quenching and reduction in persistent photoconductivity as well. This method to control optoelectrical characteristics can be used to load additional functionalities for various applications like photodetectors and gas and chemical sensors.

* Corresponding author.
E-mail address: ghkim@skku.edu (G.-H. Kim).

https://doi.org/10.1016/j.spmi.2020.106507
Received 31 December 2019; Received in revised form 26 March 2020; Accepted 1 April 2020
Available online 13 April 2020

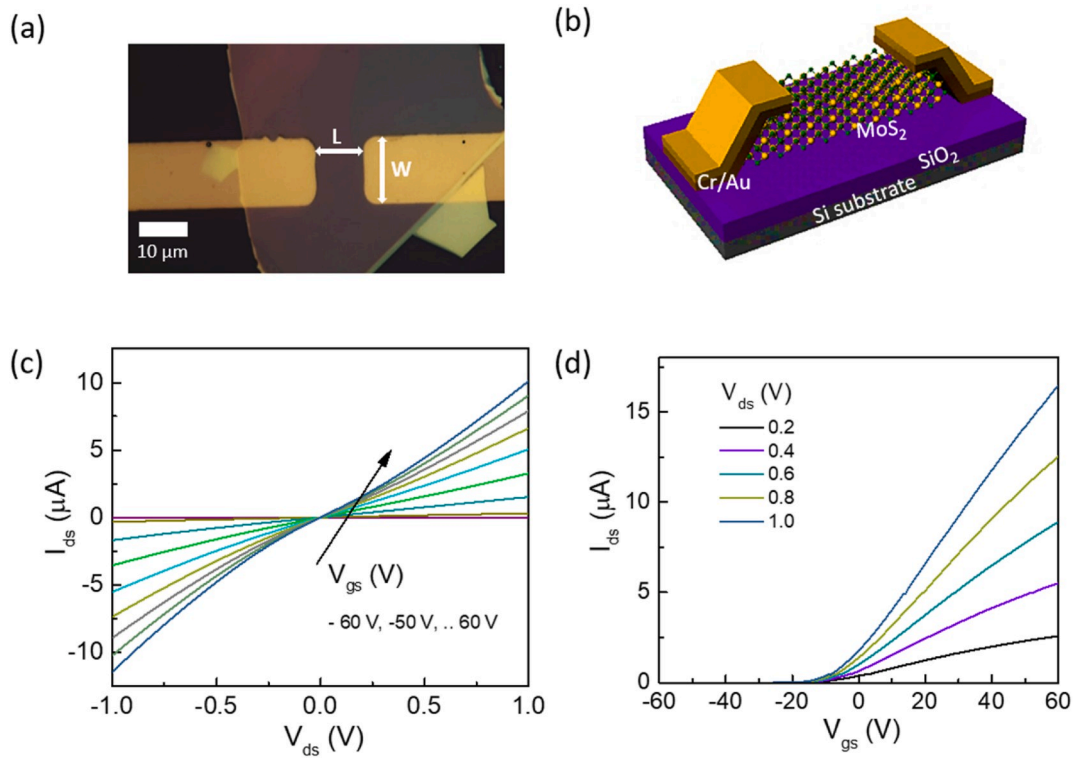

Fig. 1. (a) Microscopic image of the pristine few-layer MoS_2 device. Schematic of (b) pristine MoS_2 device on SiO_2 substrate (c) I_{ds}-V_{ds} characteristics at different gate voltages (V_{gs}) and (d) transfer characteristics at different drain voltages (V_{ds}) of the pristine device.

2. Experimental

2.1. Device fabrication and plasma treatment

The source for sample fabrication were obtained from the high-quality flake producer, 2D semiconductors [14]. The few-layer flakes were obtained by scotch tape method directly onto the SiO_2 substrates. The flakes quality and the effect of plasma exposure were measured using Raman scattering and PL techniques at room temperature. The exfoliated flakes on SiO_2 substrates were processed to fabricate MoS_2 based transistor where back gate electrode was heavily doped silicon substrate with 300 nm SiO_2 dielectric, which were cleaned in ultrasonic bath of acetone and isopropyl alcohol followed by 1-min oxygen plasma exposure for cleaning any residues. The exfoliated flakes on SiO_2/Si substrate were then processed for photolithography steps to obtain two-terminal metal contacts on the targeted flake. The contact metal, Cr/Au, was deposited to obtain Ohmic like contacts which was followed by annealing for half an hour at 300 °C in argon environment to improve contact properties [15]. The channel length and width is 10 μm and 14 μm, respectively.

The oxygen plasma treatment on the devices was carried out at 50 kHz frequency at 50 W. The exposure to plasma in treatment mode where the accelerated plasma species are not directly bombarded to the sample surface [16]. The device were exposed to plasma in the interval of 1 min followed by the measurement and subsequent plasma process in the next step. The optoelectrical measurements were carried out using Keithley 4200 SCS and the illumination of laser of 450 nm which has the power of 0.1 mW under atmospheric conditions.

3. Results and discussion

Firstly, the electrical characterization of the pristine MoS_2 FET device, as shown in Fig. 1a–b, was carried out under atmospheric conditions. Fig. 1c plots output characteristics (I_{ds} - V_{ds}) of the device for various back gate voltages. The output resistance in the order of few hundred kilo-Ohms and symmetric curves for positive and negative bias points towards the formation of Ohmic like metal contacts to MoS_2 flakes. However, the absence of I_{ds} saturation with respect to V_{ds} in the output curves indicates high contact resistance which is one of the big issues in the realization of the MoS_2 devices for commercial purposes [17,18]. Fig. 1d plots transfer characteristics (I_{ds}-V_{gs}) of the pristine device and as seen from the figure, the device shows an excellent modulation of the drain current by the back gate voltage in the drain voltage range from 0.2 V to 1.0 Various device metrics like threshold voltage, field-effect mobility (μ_e) and on-off ratio can be extracted from the transfer curves. The threshold voltage of approx. −12 V is obtained by using the method of linear extrapolation at the peak transconductance [19]. Further, the field-effect mobility can also be obtained using the following

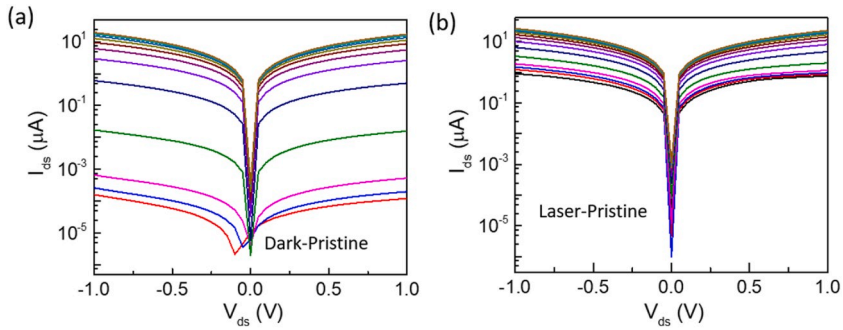

Fig. 2. Optoelectrical response of the pristine device. Output characteristics at various V_{gs} ranging from −60 V to 60 V in the step of 10 V (a) under dark conditions and (b) under laser illumination of wavelength 450 nm and power of 100 μW.

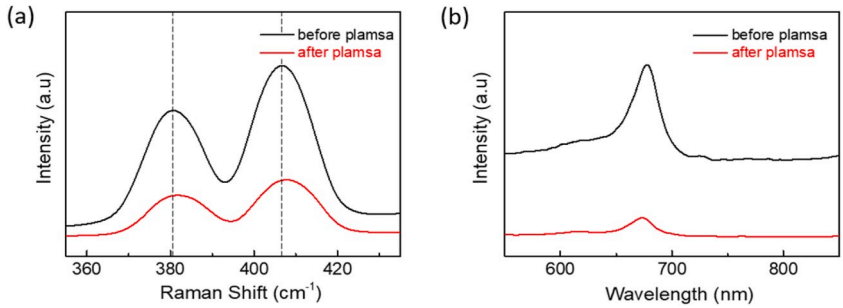

Fig. 3. Optical characterization of MoS_2. (a) Raman spectra and (b) Photoluminescence spectra of multilayer MoS_2 device before and after plasma treatment.

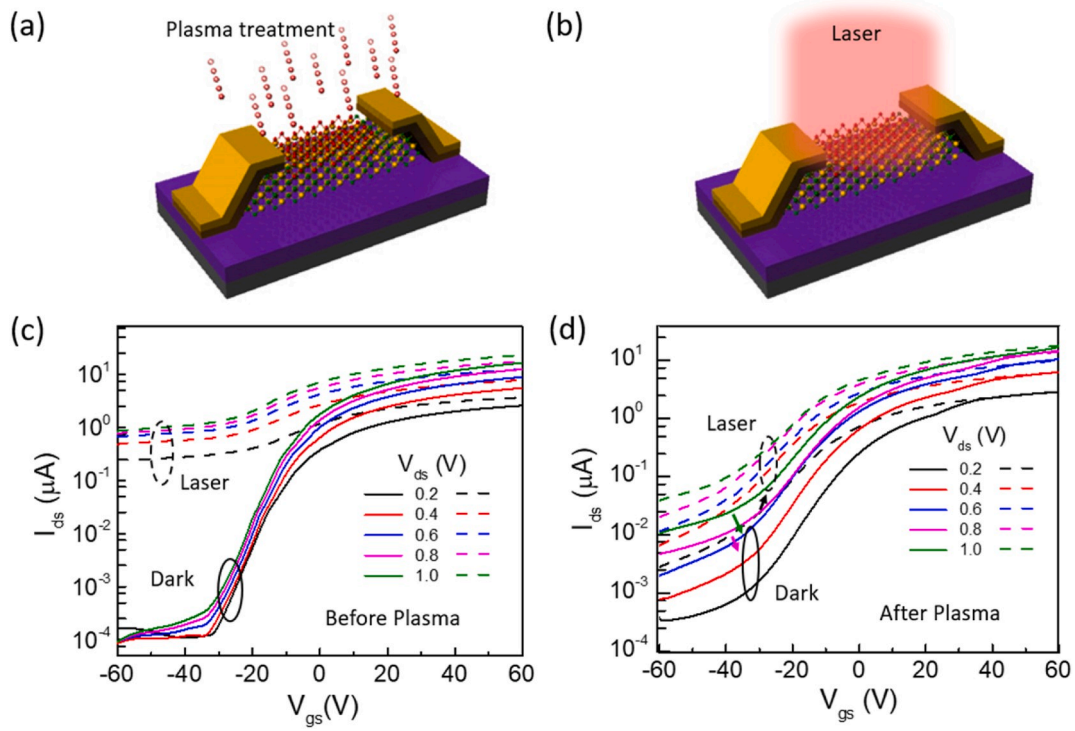

Fig. 4. (a–b) Schematic of plasma treatment and laser illumination on the devices. Transfer characteristics (I_{ds}-V_{gs}), under dark and illumination, of (c) pristine device and (d) plasma treated device at various drain voltages.

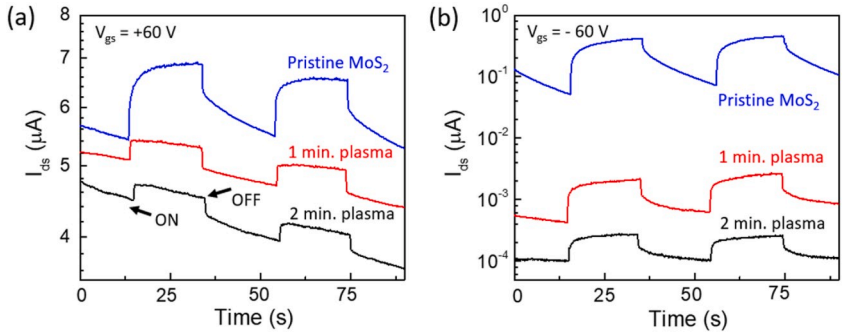

Fig. 5. (a–b) Time dependence of drain current with switching laser pulse and back gate voltage of +60 and −60 V respectively.

expression [15].

$$\mu_e = \frac{L.\ g_m}{W.\ C_{SiO_2}\ .V_{ds}}$$

where, L and W represent length and width of the channel, respectively, V_{ds} is the applied drain voltage, g_m represents the differential of the transfer curve, transconductance, where the peak value of the transconductance is usually considered for maximum field effect mobility and C_{SiO2} is capacitance per unit area which can be obtained by $\frac{\varepsilon_o \varepsilon_r}{d}$ (ε_o is the absolute permittivity and ε_r is the dielectric constant of SiO_2 of thickness d) and for 300 nm-thick SiO_2 is 1.19×10^{-8} F cm^{-2}. Using the above expression, the maximum μ_e values of the pristine devices under ambient conditions lies in the range of 20–30 cm^2/V. Various factors like contact resistance (especially in the two-terminal device configuration), flake quality, interface charge scattering at the MoS_2 and SiO_2 interface, defects and impurities in the exfoliated flakes contribute to the overall carrier mobility of the device.

Fig. 2a and b shows the opto-electrical measurement for pristine MoS_2 device. As seen from figures, the pristine device shows very good response to the illumination where the current in the OFF regime ($V_{gs} \sim$ -60 V) jumps from the order of 10^{-4} to 1 μA, whereas ON regime ($V_{gs} \sim$ +60 V) shows saturation in the optoelectrical response, which is in agreement with other published results [20].

In case of MoS_2, optical characterization methods like Raman scattering and PL are good to determine material quality and can provide additional information like number of layers, defects and band gap information, etc. Therefore, optical measurements were first carried out for exfoliated flakes and after plasma treatment process. As seen from Fig. 3a where Raman spectra of MoS_2 flake show typical signature two peaks attributed to E^1_{2g} and A_{1g} vibration modes where the peak frequencies indicate multilayers flakes [21]. As seen from the figure, the significant quenching and broadening of Raman peaks after plasma treatment indicate the increase of disorder in the crystal lattice due to oxidation by oxygen plasma [9]. This lattice distortion induced by plasma treatment is further confirmed by the quenching of A1 exciton (1.86 eV) peak as seen from the PL spectra in Fig. 3b. Such quenching have been attributed to lattice distortion and doping effects of the oxidized species generated in the plasma treatment process [9,22].

In the next step, the oxygen plasma treatment was carried out for 1 min at 50 kHz frequency and 50 W, on the fabricated MoS_2 device. Fig. 4a and b shows the schematic of plasma treatment onto the pristine device and laser illumination on the device. Fig. 4c and d plot the optoelectrical transfer characteristics of the pristine and plasma treated device. Fig. 4c agrees well with the optoelectrical response of the pristine device in Fig. 2. It can be seen from the figure that under illumination, the drain current jumps by the 4 orders of magnitude in the OFF regime whereas in the ON regime, only a slight increase in the current is observed. The current jump in the OFF regime is attributed to the generation of electron-hole pairs in the depleted MoS_2 channel under illumination which led to high drain current in the channel whereas the carrier density becomes saturated in the ON regime which limits the increase in the drain current upon illumination [23].

Fig. 4d shows the transfer characteristics of the plasma treated device both under dark and illumination. As compared to the pristine device, the overall photoresponse is reduced after plasma treatment. It can be seen that the current jump in the OFF regime is reduced to one order of magnitude whereas the photoresponse is negligible in the ON regime. This reduction in the photoresponse agrees well with the quenching of Raman scattering and PL peaks in Fig. 3. Therefore, this reduced optoelectrical response can also be attributed to the increase disorder in the lattice and the formation of oxidative species on the exposed surface of the flake. Further, it can be observed from Fig. 4 that a decrease in on-off ratio of the plasma treated device has been observed. Further, the decrease in transconductance ultimately results in the lower mobility after the plasma treatment. This can be explained from the combined effect of the carrier depletion due to formation of the oxidative species which also enhanced remote ionized or coulomb scattering thus affecting device characteristics adversely [24].

Fig. 5 plots the optoelectrical response of the pristine and plasma treated device for 1 min and 2 min duration consecutively. The time dependent behavior of optoelectrical response was measured for depletion and saturation region as well. It can be seen that at both gate voltage, the current reduces after successive plasma treatment. Further, the device characteristics appears to be stable in depletion mode as compared to less stable saturation mode which can be attributed to several affects including Joule heating induced higher conductivity at higher operating current. Further besides these adverse outcomes, the persistent photoconductivity, which is one of the critical issue in photodetectors, seems to be suppressed in the plasma treated devices due to higher and additional

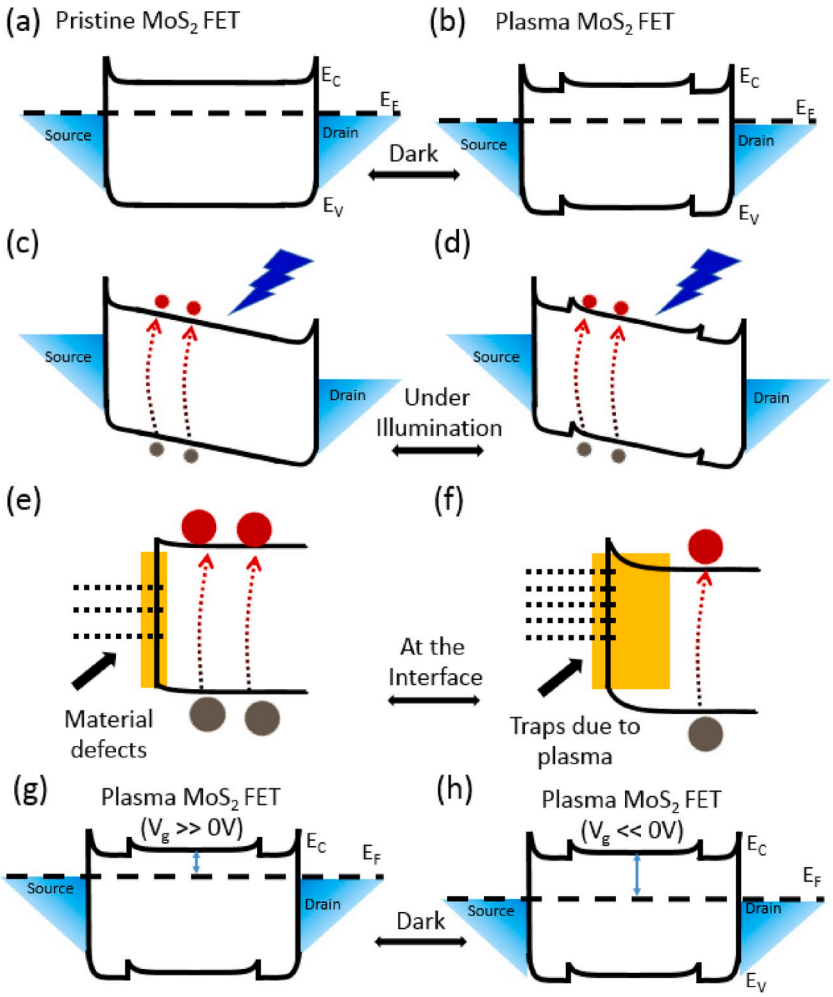

Fig. 6. (a–b) Schematics for the energy band diagram of MoS_2 device (c–d) Electron-holes generation process under applied drain bias (e–f) Illustration at the upper interface between MoS_2 layer and air showing the generation and recombination process under illumination, for pristine and plasma treated device, respectively (g–h) Illustrating the effect of gate voltage on band diagram of plasma treated MoS_2.

recombination process at the plasma induced defects [15].

This is explained further using schematic energy band diagrams in Fig. 6. Fig. 6a–c shows energy bands across source and drain under dark and illumination for both pristine and plasma treated devices. A slight barrier is shown in the plasma treated device near the source and drain contacts which indicate a possible shadow region near electrodes. The formation of oxidative species leads to carrier depletion in the channel thus upward shifting of the bands resulting in the formation of additional barriers at the electrodes which leads to higher channel resistance to carriers thus reduced drain current under both dark and illumination conditions. The recovery of persistent photoconductivity in the plasma treated devices can also be explained through the formation of additional states within the band gap which provides additional recombination path via localized states like SRH (Shockley-Read-Hall), Auger recombination, and trap/localized states assisted recombination, thus reducing the persistent photoconductivity [15,25]. Fig. 6(e–f) show the formation of traps in the device after the plasma treatment. These plamsa assisted traps are formed at the top interface of the channel and are able to capture free carriers and affect both photoconductivity and electrical characteristics of the device. So, on one hand these traps cause a reduced persistent photoconductivity behavior while on the other side leads to an increase in the leakage current via various conduction mechanism like hopping conduction, even at reduced carrier concentration in the negative gate regime. These traps are also shown in Fig. 6g and h, where at high negative gate voltage, electrons captured by traps result in conduction and flow of leakage current.

4. Conclusions

The pristine and plasma-treated few layers MoS_2 devices were characterized for optical and optoelectrical properties. Although the plasma treatment resulted in the quenching of both Raman and PL spectra but the optoelectrical characteristics maintained

approximately similar values. However, a slight decrease in drain current and corresponding photoresponse was observed after the plasma treatment, but the reduction in persistent photoconductivity was also observed. This improvement in the photo detecting properties can be optimized further by using suitable plasma power and exposure time for the specific applications like photodetectors, gas or chemical sensors.

CRediT authorship contribution statement

Muhammad Atif Khan: Methodology, Validation, Writing - original draft. **Servin Rathi:** Conceptualization, Writing - review & editing. **Sun Jin Yun:** Resources. **Gil-Ho Kim:** Supervision, Funding acquisition.

Acknowledgements

This research was supported by Basic Science Research Program through the National Research Foundation of Korea (NRF) funded by the Ministry of Education, Science and Technology (2019R1A2C2088719 and 2016R1D1A1B03932455) and Korea Research Fellowship Program through the NRF funded by the Ministry of Science, ICT and Future Planning (2015H1D3A1062519). This work was partly supported by Institute for Information & Communications Technology Promotion (IITP) grant funded by the Korea government (MSIT) (2016-00-00576, Fundamental technologies of two-dimensional materials and devices for the platform of new-functional smart devices).

Appendix A. Supplementary data

Supplementary data to this article can be found online at https://doi.org/10.1016/j.spmi.2020.106507.

References

[1] Q.H. Wang, K. Kalantar-Zadeh, A. Kis, J.N. Coleman, M.S. Strano, Nat. Nanotechnol. 7 (2012) 699.
[2] D. Voiry, A. Mohite, M. Chhowalla, Chem. Soc. Rev. 44 (2015) 2702.
[3] W. Choi, N. Choudhary, G.H. Han, J. Park, D. Akinwande, Y.H. Lee, Biochem. Pharmacol. 20 (2017) 116.
[4] N.A. Lanzillo, A. Glen Birdwell, M. Amani, F.J. Crowne, P.B. Shah, S. Najmaei, Z. Liu, P.M. Ajayan, J. Lou, M. Dubey, S.K. Nayak, T.P. O'Regan, Appl. Phys. Lett. 103 (2013) 93102.
[5] D.H. Kang, J. Shim, S.K. Jang, J. Jeon, M.H. Jeon, G.Y. Yeom, W.S. Jung, Y.H. Jang, S. Lee, J.H. Park, ACS Nano 9 (2015) 1099.
[6] C.H. Lui, A.J. Frenzel, D.V. Pilon, Y.H. Lee, X. Ling, G.M. Akselrod, J. Kong, N. Gedik, Phys. Rev. Lett. 113 (2014) 1.
[7] K.C. Chen, C.R. Wu, X.R. Chang, S.W. Chang, S.C. Lee, S.Y. Lin, Jpn. J. Appl. Phys. 55 (2016).
[8] X. Wei, Z. Yu, F. Hu, Y. Cheng, L. Yu, X. Wang, M. Xiao, J. Wang, X. Wang, Y. Shi, AIP Adv. 4 (2014), 0.
[9] N. Kang, H.P. Paudel, M.N. Leuenberger, L. Tetard, S.I. Khondaker, J. Phys. Chem. C 118 (2014) 21258.
[10] M. Chen, H. Nam, S. Wi, L. Ji, X. Ren, L. Bian, S. Lu, X. Liang, Appl. Phys. Lett. 103 (2013) 142110.
[11] M.R. Islam, N. Kang, U. Bhanu, H.P. Paudel, M. Erementchouk, L. Tetard, M.N. Leuenberger, S.I. Khondaker, Nanoscale 6 (2014) 10033.
[12] H. Nan, Z. Wang, W. Wang, Z. Liang, Y. Lu, Q. Chen, D. He, P. Tan, F. Miao, X. Wang, J. Wang, Z. Ni, ACS Nano 8 (2014) 5738.
[13] X. Wei, Z. Yu, F. Hu, Y. Cheng, L. Yu, X. Wang, M. Xiao, J. Wang, X. Wang, Y. Shi, AIP Adv. 4 (2014) 123004.
[14] M. Kang, S. Rathi, I. Lee, L. Li, M.A. Khan, D. Lim, Y. Lee, J. Park, S.J. Yun, D.-H. Youn, C. Jun, G.-H. Kim, Nanoscale 9 (2017) 1645.
[15] N. Rathi, S. Rathi, I. Lee, J. Wang, M. Kang, D. Lim, M.A. Khan, Y. Lee, G.-H. Kim, RSC Adv. 6 (2016) 23961.
[16] R. Dhall, K. Seyler, Z. Li, D. Wickramaratne, M.R. Neupane, I. Chatzakis, E. Kosmowska, R.K. Lake, X. Xu, S.B. Cronin, ACS Photonics 3 (2016) 310.
[17] S. Xu, Z. Wu, H. Lu, Y. Han, G. Long, X. Chen, T. Han, W. Ye, Y. Wu, J. Lin, J. Shen, Y. Cai, Y. He, F. Zhang, R. Lortz, C. Cheng, N. Wang, 2D Mater. 3 (2016) 21007.
[18] Y. Xu, C. Cheng, S. Du, J. Yang, B. Yu, J. Luo, W. Yin, E. Li, S. Dong, P. Ye, X. Duan, ACS Nano 10 (2016) 4895.
[19] A. Ortiz-Conde, F.J. García Sánchez, J.J. Liou, A. Cerdeira, M. Estrada, Y. Yue, Microelectron. Reliab. 42 (2002) 583.
[20] S. Rathi, I. Lee, D. Lim, J. Wang, Y. Ochiai, N. Aoki, K. Watanabe, T. Taniguchi, G.-H. Lee, Y.-J. Yu, P. Kim, G.-H. Kim, Nano Lett. 15 (2015) 5017.
[21] H. Li, Q. Zhang, C.C.R. Yap, B.K. Tay, T.H.T. Edwin, A. Olivier, D. Baillargeat, Adv. Funct. Mater. 22 (2012) 1385.
[22] U. Bhanu, M.R. Islam, L. Tetard, S.I. Khondaker, Sci. Rep. 4 (2014) 5575.
[23] J. Shim, A. Oh, D. Kang, S. Oh, S.K. Jang, J. Jeon, M.H. Jeon, M. Kim, C. Choi, J. Lee, S. Lee, G.Y. Yeom, Y.J. Song, J. Park, Adv. Mater. 28 (2016) 6985.
[24] Y. Guo, X. Wei, J. Shu, B. Liu, J. Yin, C. Guan, Y. Han, S. Gao, Q. Chen, Appl. Phys. Lett. 106 (2015).
[25] J. Shang, L. Ma, J. Li, W. Ai, T. Yu, G.G. Gurzadyan, Sci. Rep. 2 (2012) 792.